Fragile glasses induced by a dramatic drop of entropy towards the glass transition

Chun-Shing Lee[1], Matteo Lulli[1], Ling-Han Zhang[2], Hai-Yao Deng[3], and Chi-Hang Lam[1]*
[1]*Department of Applied Physics, Hong Kong Polytechnic University, Hong Kong, China*
[2]*Department of Physics, Carnegie Mellon University, Pittsburgh, Pennsylvania 15213, USA*
[3]*School of Physics and Astronomy, University of Manchester, Manchester, M13 9PL, UK*
(Dated: September 17, 2019)

We perform kinetic Monte Carlo simulations of a distinguishable-particle lattice model of structural glasses with random particle interactions. By varying the interaction distribution and the average particle hopping energy barrier, we obtain an extraordinary wide range of kinetic fragility. A stretching exponent, characterizing structural relaxation, decreases with the kinetic fragility in agreement with experiments. The most fragile glasses are those exhibiting low hopping barriers and, more importantly, dramatic drops of the entropy upon cooling towards the glass transition temperature. Quantitatively, the computed kinetic fragility is shown to increase with a thermodynamic fragility.

An important concept in the study of structural glasses [1–3] is the kinetic fragility, often simply called the glass fragility [4]. It describes how rapidly the dynamics slows down when temperature decreases. The dynamics is typically characterized by viscosity, structural relaxation time [5, 6], or particle diffusion coefficient [7, 8]. Glasses possessing the most dramatic slowdown are classified as fragile, whereas the opposite are referred to as strong. Several models of glasses have been able to reproduce a range of kinetic fragilities [9–12]. A closely related thermodynamic fragility [13] has also been defined and is based on how dramatically the entropy drops as the temperature decreases. Experimental results indicate, in general, a positive correlation between the kinetic and thermodynamic fragilities [13]. Yet, a fundamental understanding of the fragilities and their relationship is still lacking.

In this letter, we study both the kinetic and thermodynamic fragilities using a recently proposed distinguishable particles lattice model (DPLM) of structural glasses [14]. Lattice models are instrumental in statistical physics because they are often intuitively understandable and analytically tractable. The DPLM possesses exactly solvable equilibrium statistics. Computationally, it successfully reproduces typical glassy behaviors [14] as well as a remarkable phenomenon known as Kovacs' expansion gap paradox [15]. Here, we show that both the kinetic and thermodynamic fragilities of this model can be simultaneously varied over wide ranges of values via the fine-tuning of either kinetic or thermodynamic properties of the model. Specifically, the kinetic and thermodynamic properties are tuned via appropriate choices of a particle hopping energy barrier offset and a particle pair-interaction distribution respectively. Moreover, glasses thus modeled with higher kinetic fragilities in general exhibit smaller stretching exponents as well as higher thermodynamic fragilities, in good qualitative agreement with experiments. The fundamental mechanisms behind the fragility variations in this model are intuitively understandable, and are likely applicable also to realistic glasses.

We basically adopt the DPLM proposed in Ref. [14], with differences explained in Sec. I in the SI. It is defined by a 2D square lattice of size L^2 with $L = 100$ and unit lattice constant following periodic boundary conditions. There are N particles in the system which are distinguishable and numbered from 1 to N. Each site i can be occupied by one of the particles with a particle index $s_i = 1, 2, \ldots, N$. For unoccupied sites, $s_i = 0$. A void density of $\phi_v = 0.01$ is considered. A particle configuration is specified by the set of particle indices $\{s_i\}$ over all sites. The total system energy is

$$E = \sum_{\langle i,j\rangle'} V_{s_i s_j}, \tag{1}$$

where the sum is restricted to nearest neighboring (NN) sites i and j occupied by particles. Each interaction V_{kl} for each particle pair k and l is sampled before the start of the simulation from the pair-interaction distribution $g(V_{kl})$. The particle index s_i at site i is time dependent since the site will be visited by different particles as the system evolves. Thus, $V_{s_i s_j}$ in Eq. (1) is time dependent, although any V_{kl} for any given particles k and l is quenched. Particle distinguishability and particle-dependent interactions are readily justifiable for polydispersive or polymer systems, while they effectively account for the generally different frustration states experienced by the particles for identical particle systems. It also models high-entropy alloys in the glassy state [16] in the limit of a large number of atomic species. Being a lattice model, particle vibrations are not explicitly accounted for. A particle configuration more precisely models an inherent state in a realistic system [17].

A main feature of our work is the random sampling of each $V_{kl} \in [V_0, V_1] \equiv [-0.5, 0.5]$ from a *bi-component distribution* consisting of a uniform and a delta function given by

$$g(V) = \frac{G_0}{\Delta V} + (1 - G_0)\delta(V - V_1), \tag{2}$$

* Email: C.H.Lam@polyu.edu.hk

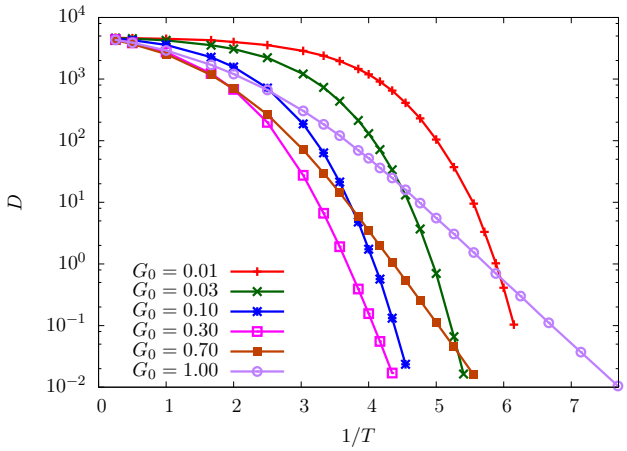

Figure 1. Arrhenius plot of D for various G_0 at $E_0 = 0$. The system with a lower G_0 is more super-Arrhenius.

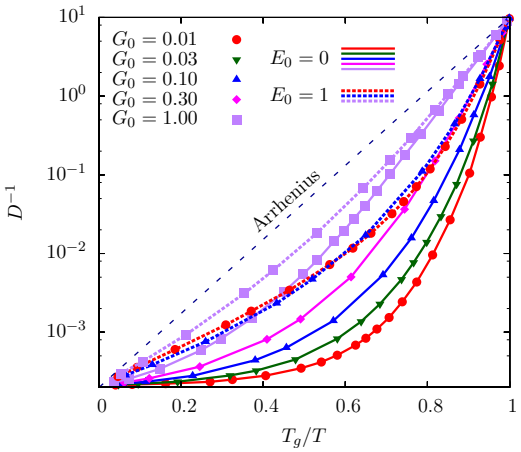

Figure 2. Kinetic Angell plot of D^{-1} against T_g/T for various G_0 and E_0, where T_g for each curve is defined at $D_r = 10^{-1}$. A low G_0 gives a fragile system. For a given G_0, increasing E_0 makes the system stronger.

where $\Delta V = V_1 - V_0 = 1$ and δ denotes the Dirac delta function. Here, $G_0 \in [0, 1]$ is our main thermodynamic parameter controlling the fragilities. It equals the probabilistic weight of the uniform component of the distribution and also the probability density $g(V_0)$ at the ground state energy V_0. For $G_0 = 1$, Eq. (2) reduces to the uniform distribution used in Ref. [14], which leads to a strong glass. Alternatively, for $G_0 = 0$, the model reduces to a simple identical-particle lattice gas with a uniform particle interaction.

The dynamics is defined by the standard Metropolis algorithm. At temperature T, each particle can hop to an unoccupied NN site at a rate

$$w = \begin{cases} w_0 \exp\left[-\left(E_0 + \Delta E\right)/k_B T\right] & \text{for } \Delta E > 0 \\ w_0 \exp\left(-E_0/k_B T\right) & \text{for } \Delta E \le 0 \end{cases} \quad (3)$$

where ΔE is the change in the system energy E given by Eq. (1) due to the hop. We also put $w_0 = 10^6$ and $k_B = 1$ is the Boltzmann constant. The hopping energy barrier offset $E_0 \ge 0$ is our main kinetic model parameter for controlling the fragilities. Our algorithm satisfies detailed balance.

Based on the DPLM explained above, kinetic Monte Carlo simulations have been performed, starting from directly constructed initial equilibrium configurations as explained in Ref. [14]. We report here our main results while further details are given in Sec. II in the SI. The particle mean squared displacement defined as MSD $= \left\langle |\mathbf{r}_l(t) - \mathbf{r}_l(0)|^2 \right\rangle$ is calculated, where $\mathbf{r}_l(t)$ denotes the position of particle l at time t. The average is performed over all particles and over five independent samples. Examples of results are shown in Fig. S1. In $d = 2$ dimensions, the particle diffusion coefficient D is computed according to $D = (1/2d)\,(\mathrm{MSD}/t)$ at sufficiently large values of t in the diffusion regime.

The Arrhenius plot in Fig. 1 shows D against $1/T$ for $E_0 = 0$ and various G_0. We observe that $\log D$ decreases with $1/T$ faster than linearly, demonstrating a super-Arrhenius slowdown. The dependence of D on G_0 for any given T is non-monotonic. Yet, the super-Arrhenius behavior strengthens monotonically as G_0 decreases. This can be clearly seen in a *kinetic* Angell plot in Fig. 2 which plots D^{-1} against T_g/T for $E_0 = 0$ (solid lines) using the data from Fig. 1. We have defined the glass transition temperature T_g as T at which $D = D_r \equiv 10^{-1}$, where the reference diffusion coefficient D_r is about the lowest value we can simulate. We observe that D now varies monotonically with G_0 for any given T_g/T. More importantly, the super-Arrhenius property clearly strengthens monotonically as G_0 decreases. Figure 2 also shows D^{-1} for $E_0 = 1$ (dotted lines). Results are simply obtained from values of D for $E_0 = 0$ after rescaling time by a factor $\exp\left(E_0/k_B T\right)$, noting that T_g has to be recalculated since D_r is not rescaled. We observe that a smaller E_0 strengthens the super-Arrhenius property at any given G_0.

The kinetic fragility m_k describes the super-Arrhenius property quantitatively and is defined by $m_k = \partial \log D^{-1}/\partial(T_g/T)|_{T=T_g}$. Figure S4 plots m_k against G_0 for $E_0 = 0, 0.5, 1$. We obtain a wide range of values of m_k from 4.70 to 26.35, reaching a maximum fragile-to-strong ratio 5.62. This ratio is comparable to the ratio 6 for typical m_k from 25 to 150 in experiments [18]. Values of m_k obtained here are in general smaller than experimental values, but this is only due to a rather small D_r adopted for defining T_g. A rough extrapolation to $D_r = 10^{-14}$ is done (see Sec. III in the SI), so that 17 orders of magnitude of D are considered, similar to analyses of τ and η in experiments [5, 6]. After extrapolation, the range of m_k is consistent with the experimental range.

To further establish the physical relevance of the model, we next show that relaxation and thermodynamic properties of the strong and fragile glasses from the DPLM are consistent with experimental trends. First, structural relaxation is studied by measuring the self-

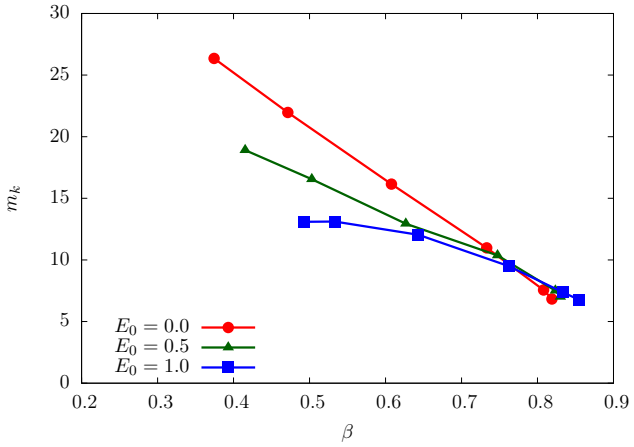

Figure 3. Relationship between m_k and β at $E_0 = 0, 0.5, 1$ with $G_0 = 0.01, 0.03, 0.1, 0.3, 0.7, 1$ (from left to right).

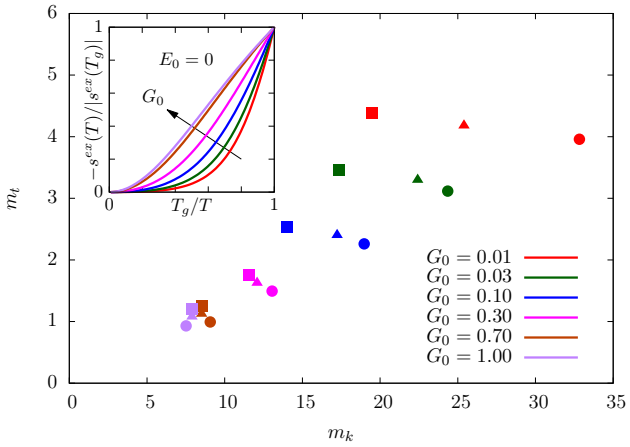

Figure 4. Plot of m_t against m_k at $E_0 = 0$ (circle), 0.5 (triangle), 1 (square) for various G_0. Inset: Angell plot of $-s^{ex}(T)/|s^{ex}(T_g)|$ at $E_0 = 0$.

intermediate scattering function

$$F_s(\mathbf{q}, t) = \left\langle e^{i\mathbf{q}\cdot(\mathbf{r}_l(t)-\mathbf{r}_l(0))} \right\rangle, \tag{4}$$

where $q = (2\pi/L)q'$ with $q' = 10$. Results at $G_0 = 0.01$ and low T are shown in Fig. S2 and they can be nicely fitted by the stretched exponential function $A\exp(-(t/\tau)^\beta)$ for $t \gtrsim \tau$, where β, τ and A are respectively the stretching exponent, the relaxation time, and a constant close to unity. We plot β against T_g/T for various G_0 in Fig. S3. Figure 3 plots m_k against β at T_g for various G_0 and E_0. It shows that m_k tends to decrease approximately linearly with β, in agreement with a trend observed previously in experiments [18]. In addition, the obtained range 0.37 to 0.81 of β is comparable to that from experiments. Results regarding β are not significantly affected by using different values of D_r, especially for the fragile glasses since T_g only changes slightly.

Second, we study the thermodynamic properties of our model by calculating an entropy-based *thermodynamic fragility*. The equilibrium statistics including the partition function Z of the DPLM are exactly known [14]. The entropy per particle $s(T)$ is computed accordingly. We further define an excess entropy per particle $s^{ex}(T) = s(T) - s^{LG}$ over the entropy s^{LG} of a simple lattice gas [19]. (Detailed calculations are reported in Sec. IV of the SI with the complete expression of $s^{ex}(T)$ given in Eq. (S10).) The inset of Fig. 4 shows a *thermodynamic* Angell plot of $-s^{ex}(T)/|s^{ex}(T_g)|$ against T_g/T for $E_0 = 0$ and different G_0. The results resemble those of the closely related thermodynamic Angell plots from experiments [20] as well as the kinetic Angell plot in Fig. 2. An increased E_0 enhances the curvature only slightly for all values of G_0 (results not shown). In general, a strong glass with $G_0 = 1$ is also thermodynamically strong with a close-to-linear relation, while a fragile glass at $G_0 = 0.01$ shows the most dramatic variations. The trend is in general similar if other forms of thermodynamic Angell plots [20] are considered.

We define a thermodynamic fragility m_t as

$$m_t = \left. \frac{\partial\left(-s^{ex}(T)/|s^{ex}(T_g)|\right)}{\partial\left(T_g/T\right)} \right|_{T=T_g}, \tag{5}$$

which is analogous to the kinetic counterpart m_k. A plot of m_t against G_0 for various values of E_0 is shown in Fig. S5. Finally, Fig. 4 shows the kinetic fragility m_t against the thermodynamic fragility m_k for various G_0 and E_0, displaying a clear tendency of a positive correlation, i.e. $m_t \sim m_k$. The correlation is consistent with the general trend observed in experiments based on related definitions [20] and results mainly from the similar dependencies of m_k and m_t on G_0.

We have studied glass fragility using the DPLM for various values of model parameters G_0 and E_0. The most fragile glass is obtained at small G_0 and $E_0 = 0$. Extrapolating our simulation results towards $G_0 \to 0$, the kinetic fragility m_k appears to rise unboundedly (see Fig. S4 in SI). The DPLM may hence model in-principle arbitrarily fragile glasses. Simulations at very small G_0 are however prohibitively intensive due to increased finite-size effects. At $G_0 = 0$, the model reduces to a simple lattice gas, which is not glassy. A high m_k thus requires a small but non-vanishing probability of low-energy particle pairings.

Intuitively, a fragile glass obtained at a small G_0 can be easily understood as follows. At high T, all particle configurations are possible leading to a high entropy $s(T)$ independent of G_0. As T decreases, a small G_0 implies that only a rare population of particle pairings are energetically favorable. The entropy $s(T)$ thus drops dramatically and become small at low T, accounting for a high m_t. The rarity of energetically favorable configurations also implies highly constrained kinetic pathways of particle motions. There is thus an associated sharp drop in D described by a large m_k.

The particle interaction distribution $g(V)$ has been

taken as a bi-component form consisting of a low-energy uniform distribution and a high-energy delta function for simplicity. The delta function represents typical particle interactions and replacing it by some narrow Gaussian leads to similar simulation results. The uniform distribution is the simplest continuous distribution with a lower bound V_0, corresponding to the energy minimum present in typical pair potentials such as the Lennard-Jones potential. The continuous form of $g(V)$ around V_0 is expected to lead to glassy behaviors even at a very low T, as the model reduces to one with a single uniform distribution studied in Ref. [14]. Alternatively, by adding a delta function at V_0 in Eq. (2), the model reduces at very low T to a lattice gas constrainted to a subset of allowed particle pairings, which is expected to be non-glassy. This may realize a low temperature fragile-to-strong transition [21] and will be studied in the future.

The DPLM with a bi-component $g(V)$ is closely related to a two-state model proposed in Ref. [22], in which particle bonds can take either an unexcited or excited state (see Sec. IV in SI). At low T, the realized interactions $V_{s_i s_j}$ from the uniform component have a small energy spread of about k_BT around $V_0 + k_BT$. Neglecting this energy spread, the ratio of the degeneracy of the high-energy (i.e. excited) to that of the low-energy (i.e. unexcited) is about $(1-G_0)/G_0$, leading to an entropy difference $\Delta S^0 \simeq k_B \ln[(1-G_0)/G_0]$. Consider $G_0 = 0.01$ corresponding to fragile glasses, and we get $\Delta S^0 \simeq 4.6 k_B$. A more accurate calculation using Eq. (S29) gives a similar value of $\Delta S^0 \simeq 5.42 k_B$. Using $k_B = 8.315$ J/mol·K, it gives $\Delta S^0 \simeq 45.1$ J/K per mole of excitable states. This value matches that of ΔS^0 for example for toluene in Ref. [22], which has a high $m_k = 103$. In addition, $\Delta H^0/k_BT_g \simeq (1-0.163)/0.163 \simeq 5.15$ for $G_0 = 0.01$ in our model, where $\Delta H^0 \simeq 1 - k_BT_g$ is the energy difference between the excited and unexcited states taken at $T_g \simeq 0.163$. It compares well with the value 6.95 for toluene Ref. [22]. The quantitative consistency means that the two-state model essentially provides a simplified theoretical description for the thermodynamic properties of the DPLM with the bi-component $g(V)$. Moreover, the success of the two-state model in describing the entropy of fragile glasses in Ref. [22] justifies the bi-component form of $g(V)$ used in this work.

We have found that the thermodynamic parameter G_0 has the strongest impacts on both m_k and m_t. In contrast, the kinetic parameter E_0 also plays a significant role for m_k but not so much for m_t. Further simulations show that the void density ϕ_v has rather small effects on both m_k and m_t. One can also consider model variations such as other parametrized forms of $g(V)$. Since the glass properties depend on multiple model parameters, the relations discussed here between m_k, m_t and β are only general trends assuming small variations in other parameters. Exceptions are thus possible in more general settings, as observed in experiments. Similarly, the value of m_k does not uniquely determine the precise geometry of the whole curve in the Angell plot in Fig. 2, as more than one parameter are allowed to vary. This is fully consistent with experimental observations [4].

To sum up, we have studied fragility properties of glasses using kinetic Monte Carlo simulations and analytic calculations based on the DPLM. A wide range of values of kinetic fragility is reproduced, indicating the possibility of arbitrarily fragile glasses limited only by computational resources. The kinetic fragility is mainly controlled via a thermodynamic parameter G_0, dictating the probability distribution of particle pair interactions. The most fragile glass is obtained at small G_0 corresponding to the case that pair interactions can take low-energy states with a low but non-vanishing probability, i.e. low-entropy low-energy states. These configurations physically represent rare pairings between particles with exceptionally stable arrangements. As the temperature decreases, particle configurations are increasingly constrained to these low-energy pairings. This causes a dramatic drop in the entropy and thus also a dramatic slowdown in the dynamics, resulting respectively in high thermodynamic and kinetic fragilities. Our model, upon variations in G_0, exhibits correlations between kinetic fragility, thermodynamic fragility and a relaxation stretching exponent, in qualitative agreement with general trends observed in experiments. The kinetic fragility is also affected by a kinetic model parameter E_0. A fragile glass is obtained at small E_0 corresponding to barriers with an average which is compared to their fluctuations.

We thank the support of Hong Kong GRF (Grant 15330516) and PolyU (Grants 1-ZVGH and G-UAF7).

[1] L. Berthier and G. Biroli, "Theoretical perspective on the glass transition and amorphous materials," Rev. Mod. Phys. **83**, 587 (2011).
[2] J. P. Garrahan, P. Sollich, and C. Toninelli, "Kinetically constrained models," in Dynamical Heterogeneities in Glasses, Colloids and Granular Media, edited by L. Berthier, G. Biroli, J.-P. Bouchaud, L. Cipelletti, and W. van Saarloosand (Oxford University Press, 2011).
[3] F. H. Stillinger and P. G. Debenedetti, "Glass transition thermodynamics and kinetics," Annu. Rev. Condens. Matter Phys. **4**, 263 (2013).
[4] C. A. Angell, "Formation of glasses from liquids and biopolymers," Science **267**, 1924 (1995).
[5] C. A. Angell, "Relaxation in liquids, polymers and plastic crystals strong/fragile patterns and problems," J. Non-Cryst. Solids **131-133**, 13 (1991).
[6] C. Alba, L. E. Busse, D. J. List, and C. A. Angell, "Thermodynamic aspects of the vitrification of toluene, and xylene isomers, and the fragility of liquid hydrocarbons," J. Chem. Phys. **92**, 617 (1990).
[7] F. Fujara, B. Geil, H. Sillescu, and G. Fleischer, "Translational and rotational diffusion in supercooled orthoter-

phenyl close to the glass transition," Z. Phys. B **88**, 195 (1992).
[8] D. Coslovich and G. Pastore, "Understanding fragility in supercooled lennard-jones mixtures. i. locally preferred structures," J. Chem. Phys. **127**, 124504 (2007).
[9] J. P. Garrahan and D. Chandler, "Geometrical explanation and scaling of dynamical heterogeneities in glass forming systems," Phys. Rev. Lett. **89**, 035704 (2002).
[10] F. Sausset, G. Tarjus, and P. Viot, "Tuning the fragility of a glass-forming liquid by curving space," Phys. Rev. Lett. **101**, 155701 (2008).
[11] A. Parmar and S. Sastry, "Kinetic and thermodynamic fragilities of square well fluids with tunable barriers to bond breaking," J. Phys. Chem. B **119**, 11243 (2015).
[12] O. Misaki, K. Kang, and M. Kunimasa, "Tuning pairwise potential can control the fragility of glass-forming liquids: from a tetrahedral network to isotropic soft sphere models," J. Stat. Mech. **2016**, 074002 (2016).
[13] C. A. Angell and K. Ueno, "Soft is strong," Nature **462**, 45 (2009).
[14] L.-H. Zhang and C.-H. Lam, "Emergent facilitation behavior in a distinguishable-particle lattice model of glass," Phys. Rev. B **95**, 184202 (2017).
[15] M. Lulli, C.-S. Lee, H.-Y. Deng, C.-T. Yip, and C.-H. Lam, arXiv:1909.03685 (2019).
[16] J.-W. Yeh, "Alloy design strategies and future trends in high-entropy alloys," JOM **65**, 1759 (2013).
[17] H.-Y. Deng, C.-S. Lee, M. Lulli, L.-H. Zhang, and C.-H. Lam, "Configuration-tree theoretical calculation of the mean-squared displacement of particles in glass formers," J. Stat. Mech. **2019**, 094014 (2019).
[18] M. Matthieu, "Relaxation and physical aging in network glasses: a review," Rep. Prog. Phys. **79**, 066504 (2016).
[19] J. C. Dyre, "Perspective: Excess-entropy scaling," J. Chem. Phys. **149**, 210901 (2018).
[20] L. M. Martinez and C. A. Angell, "A thermodynamic connection to the fragility of glass-forming liquids," Nature **410**, 663 (2001).
[21] R. Shi, J. Russo, and H. Tanaka, "Origin of the emergent fragile-to-strong transition in supercooled water," Proc. Natl. Acad. Sci. **115**, 9444 (2018).
[22] C. T. Moynihan and C. A. Angell, "Bond lattice or excitation model analysis of the configurational entropy of molecular liquids," J. Non-Cryst. Solids **274**, 131 (2000).

Fragile glasses induced by a dramatic drop of entropy towards the glass transition

Chun-Shing Lee[1], Matteo Lulli[1], Ling-Han Zhang[2], Hai-Yao Deng[3], and Chi-Hang Lam[1]*
[1]*Department of Applied Physics, Hong Kong Polytechnic University, Hong Kong, China*
[2]*Department of Physics, Carnegie Mellon University, Pittsburgh, Pennsylvania 15213, USA*
[3]*School of Physics and Astronomy, University of Manchester, Manchester, M13 9PL, UK*
(Dated: September 17, 2019)

I. MODEL DETAILS: DIFFERENCES FROM PREVIOUS DEFINITION

We now provide further details of the DPLM adopted in this work, focusing on the differences of this variant with respect to that in Ref. [1]. A main feature in this work is to study a bi-component form of the pair-interaction energy distribution $g(V)$, generalizing a simple uniform distribution used in Ref. [1]. This has been discussed in the main text. Here, we explain other differences.

Particle-dependent interactions: In this work, we consider a particle-dependent interaction V_{kl} between nearest neighboring (NN) particles, which depends only on the particle labels k and l (see Eq. (1) of the main text). This is a simplification from Ref. [1] which uses a particle-site-dependent interaction V_{ijkl} with additional explicit dependences on the sites i and j at which particles k and l are located. In Ref. [1], the explicit site dependence was introduced to model different frustration states at difference sites. It was already shown in Ref. [1] that the same exact equilibrium statistics hold for both V_{ijkl} and V_{kl} types of interactions. We have verified that adopting either V_{ijkl} or V_{kl} gives qualitatively similar features for all numerical measurements reported in Ref. [1] and in this work. Only minor quantitative differences are observed in general.

Although both V_{ijkl} and V_{kl} interaction types should in principle be applicable in this work, the computation for the case of V_{ijkl} is more intensive and is thus not adopted. Specifically, the whole set of V_{ijkl} requires a computer storage of size $\sim N^3 \sim L^6$, for the case of N particles in a nearly fully occupied lattice of linear size L. Using a two-step interaction energy tabulation approximation, the requirement reduces to a manageable size of $\sim N^2$. This approximation has been verified to be accurate for $G_0 = 1$ in particular by checking that the system energy E measured from simulations agrees with an exact theoretical value [1]. However, we find in this work that the accuracy deteriorates for any given L as G_0 decreases. For example, for $G_0 = 0.01$, $L = 100$ and $T = 0.22$, the measured E deviates by about 18% from the theoretical value. The error reduces if a larger L is used, but memory requirements may then be too demanding. In contrast, using V_{kl} for the same conditions, the discrepancy in E decreases to only about 0.6%. The memory consumption to store the whole set of V_{kl} is also of a manageable size of $\sim N^2$ without needing the two-step interaction energy tabulation approximation.

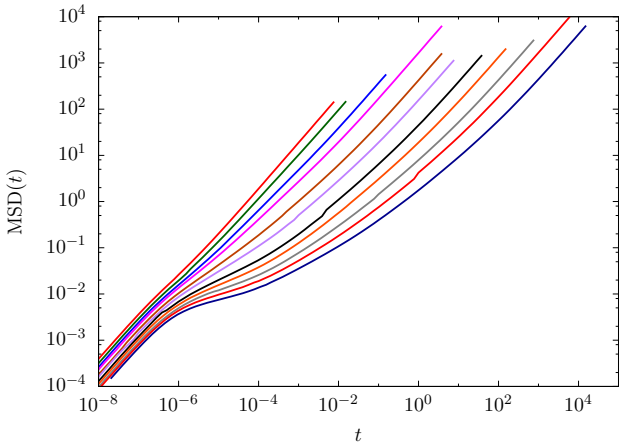

Figure S1. MSD(t) against t at $G_0 = 0.01$ and $E_0 = 0$. Different curves represent different $T = 4, 0.3, 0.24, 0.22, 0.2, 0.19, 0.18, 0.175, 0.17, 0.1667, 0.1626$ (from left to right).

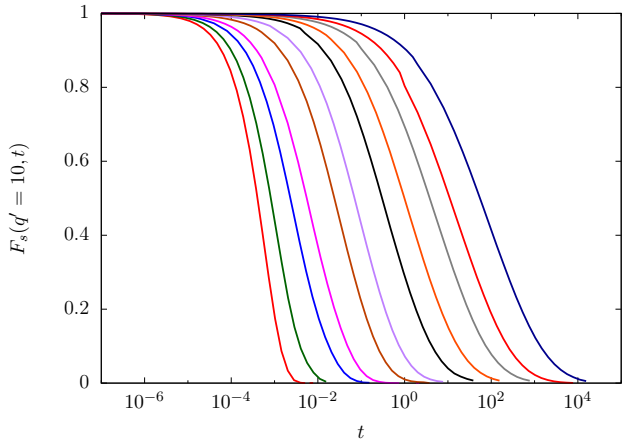

Figure S2. $F_s(\mathbf{q}, t)$ against t at $G_0 = 0.01$ and $E_0 = 0$ with $q' = 10$. Different curves represent different temperatures at $T = 4, 0.3, 0.24, 0.22, 0.2, 0.19, 0.18, 0.175, 0.17, 0.1667, 0.1626$ (from left to right).

* Email: C.H.Lam@polyu.edu.hk

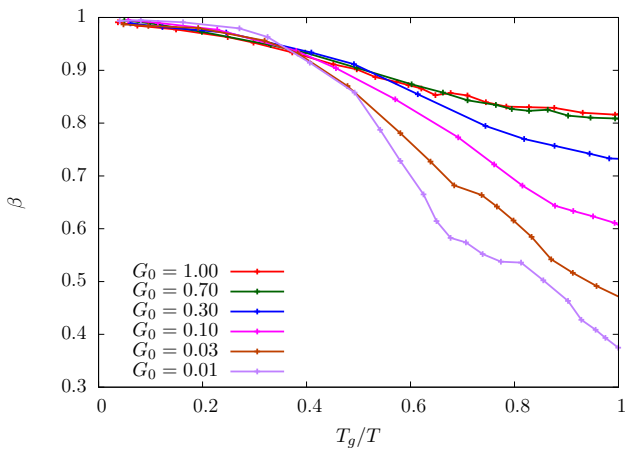

Figure S3. β against T_g/T at $G_0 = 0.01, 0.03, 0.1, 0.3, 0.7, 1$. T_g is extracted at $D_r = 0.1$ for $E_0 = 0$.

Metropolis algorithm: We apply a Metropolis form of the particle hopping rate w in Eq. (3) with a hopping energy barrier $E_0 + \max\{\Delta E, 0\}$, where ΔE is the energy change of the system induced by the hop attempt and E_0 is an energy barrier offset. The energy barrier must be non-negative in all cases and this requires $E_0 \geq 0$. In Ref. [1], an activated-hopping form of the hopping rate was used instead. A similar enforcement of the non-negativity of the energy barriers leads to a constraint $E_0 \geq 1.5$ for an analogously defined offset E_0. Both the Metropolis and the activated hopping algorithms are widely used dynamics and both satisfy detailed balance. Nevertheless, an offset of $E_0 = 0$, possible for the Metropolis algorithm, corresponds to the case of a small average barrier or equivalently large barrier fluctuations. We have found in this work that this is the regime in which the most fragile glass can be obtained. The Metropolis form is thus adopted to realize a wider range of fragilities. Interestingly, our results suggest that very fragile glasses have large fluctuations in the particle hopping energy barriers, which may be more consistent with the Metropolis function than the activated hopping function.

II. DETAILED SIMULATION RESULTS

Figure S1 shows our kinetic Monte Carlo simulation results on the mean square displacement MSD(t) versus t for the example of a fragile glass at $G_0 = 0.01$ and $E_0 = 0$. At each T, we extract the diffusion coefficient D from $D = (1/2d)\,(\mathrm{MSD}/t)$ with $d = 2$ at sufficiently large t in the diffusive regime. Specifically, we require that t is large enough to ensure that MSD > 1 and MSD $\propto t^\gamma$ with $0.95 \leq \gamma \leq 1$. For other values of G_0, the MSD is similarly measured and all data for D are shown in Fig. 1 in the main text.

From Fig. S1, we observe the emergence of a plateau characteristic of glasses as T decreases. The system is deeply supercooled at the lowest T studied, despite the rather shallow plateau which is typical for lattice models and is due to the lack of vibrations. The MSD for the example of a strong glass has been shown in Ref. [1]. Compared with a strong glass, the fragile glass in Fig. S1 exhibits a much more stretched-out plateau at low T.

Figure S2 shows the self-intermediate scattering function $F_s(\mathbf{q}, t)$ [1] computed from our simulations also for the fragile case at $G_0 = 0.01$ and $E_0 = 0$, where $\mathbf{q} = (2\pi/L)q'$ with $q' = 10$. Very stretched-out relaxation is also observable at low T. For example, the relaxation causing $F_s(\mathbf{q}, t)$ to drop from 0.9 to 0.1 covers about three decades in time for the lowest T studied. Compared with results for a strong glass illustrated in Ref. [1], the decay in Fig. S2 for the fragile glass is significantly more stretched out.

Moreover, $F_s(\mathbf{q}, t)$ in Fig. S2 shows apparently a single-step relaxation, which is indeed a two-step relaxation with a tiny first drop only noticeable upon magnification or in a semi-log scale, similar to the strong glass cases in Ref. [1]. A small first relaxation step is again typical of lattice models due to the lack of vibrations. The main relaxation is well fitted by the Kohlrausch-Willianms-Watts (KWW) stretched exponential function $A\exp(-(t/\tau)^\beta)$ at sufficiently large t beyond the first relaxation step. Here, β is the stretching exponent while τ and $A \simeq 1$ are the relaxation time and the decay magnitude of the main relaxation. Specifically, we extract β from the fit around $F_s(\mathbf{q}, t) = 1/e$. For other values of G_0, values of β are similarly obtained.

We have performed independent simulations for different values of T and G_0 primarily for $E_0 = 0$ as discussed above. Results for other values of $E_0 > 0$ can be trivially obtained from those at $E_0 = 0$ by rescaling time by a factor $\exp(E_0/k_BT)$, without performing further simulations. The diffusion coefficient D at $E_0 > 0$ is simply obtained by multiplying the corresponding value of D for $E_0 = 0$ by a factor $\exp(-E_0/k_BT)$. Note that we define T_g as T at which $D = D_r \equiv 0.1$, where the reference D_r remains a constant admitting no rescaling. As D is rescaled, T_g is varied and is recalculated from $D = D_r$. Results on D and T_g accordingly calculated for various E_0 are applied in Fig. 2 in the main text. On the other hand, while the time rescaling alters $F_s(\mathbf{q}, t)$, it does not affect β for any fixed T. Therefore, the value of β at T_g depends on E_0 only via T_g. Figure S3 shows the plot of β against T_g/T for all values of G_0 at $E_0 = 0$. Using these and similar results for $E_0 > 0$, we perform third-order polynomial fits to the dependence of β on T_g/T to provide the best estimate of β at T_g, which are used in Fig. 3 in the main text.

We have calculated the kinetic and thermodynamic fragilities m_k and m_t for various values of G_0 and E_0. Results are shown in Figs. S4 and S5 respectively. We observe empirically that for $G_0 \lesssim 0.7$, both m_k and m_t decrease linearly with $\log G_0$. Furthermore, m_k increases significantly as E_0 decreases for small G_0. Otherwise, for

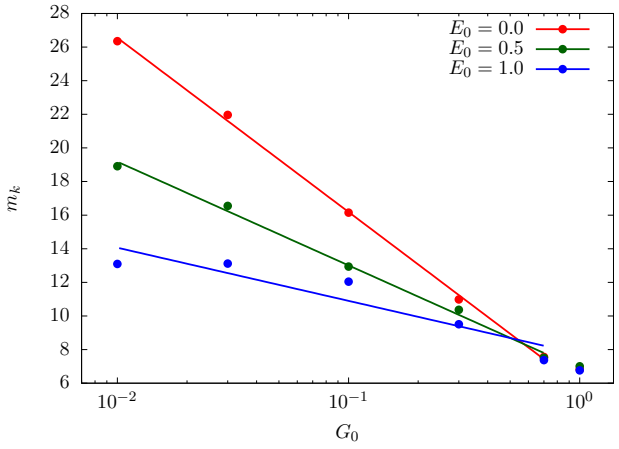

Figure S4. m_k against G_0 at $E_0 = 0, 0.5, 1$. m_k is computed at $D_r = 0.1$.

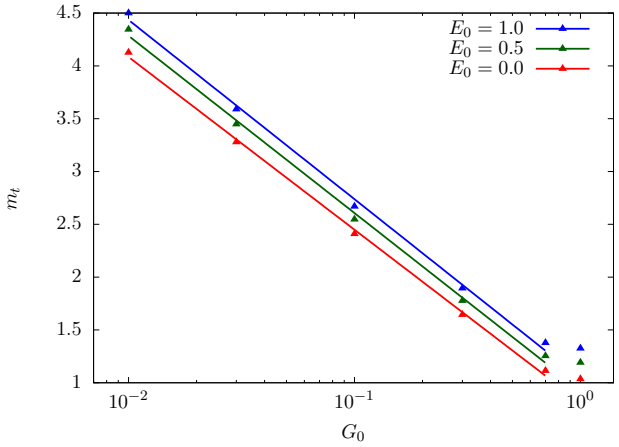

Figure S5. m_t against G_0 at $E_0 = 0, 0.5, 1$. m_t is computed at T_g at which $D_r = 0.1$.

m_t and m_k at large G_0, the dependence on E_0 is weak. Combining the results in Figs. S4 and S5, we obtain the plot of m_t against m_k in Fig. 4 in the main text.

III. KINETIC FRAGILITY EXTRAPOLATED TO REALISTIC TIME SCALE

Experimental values of the kinetic fragility m_k range typically from about 25 to 150 [2]. Values from our simulations are in contrast a few times smaller. Nevertheless, this is only because we have adopted a large reference diffusion coefficient $D_r = 0.1$ in the definition of T_g because of computational limitations. In fact, similar to all microscopic particle simulations, our DPLM simulations are limited to very short physical time scales compared with experimental situations. Adopting a much smaller D_r in direct analysis of simulations is not feasible because the required simulations would involve much slower dynamics. Here, we show that by extrapolating to a realistic value of D_r, corresponding to a much longer time scale, the obtained values of m_k increase significantly and are consistent with the typical experimental range.

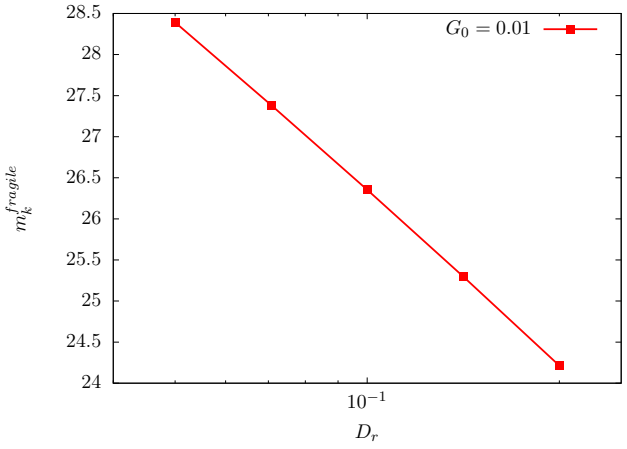

Figure S6. Kinetic fragility $m_k^{fragile}$ against D_r for $G_0 = 0.01$ and $E_0 = 0$.

We compute

$$m_k = \left. \frac{\partial \log D^{-1}}{\partial (T_g/T)} \right|_{T=T_g} \tag{S1}$$

numerically from the values of D close to T_g. We define T_g as the temperature at which $D = D_r$ with $D_r = 0.1$. Let us first consider the strong glass limit corresponding to the Arrhenius dynamics with the smallest possible kinetic fragility m_k^{strong}. As $T \to \infty$, the model reduces to a simple lattice gas. The diffusion coefficient is $D_\infty \simeq (z-2) w_0 \phi_v / 2d \simeq 5 \times 10^3$ for small ϕ_v, with the coordination number $z = 2d$ and dimension $d = 2$ [3]. Assuming an Arrhenius T dependence of D, Eq. (S1) gives $m_k^{strong} = \log(D_\infty / D_r) \simeq 4.70$. This is close to $m_k = 6.76$ for the strongest glass we have considered at $G_0 = 1$ and $E_0 = 1$ in the main text. We next consider a more realistic value of $D_r = 10^{-14}$. This value is chosen so that as T varies from T_g to ∞, D varies by nearly 18 orders of magnitude, a variation comparable to typical experimental ranges [4, 5]. This gives $m_k^{strong} = 21.4$, which is consistent with experimental values for strong glasses.

For the case of fragile glasses, we have obtained a large kinetic fragility $m_k^{fragile}$ at $G_0 = 0.01$ and $E_0 = 0$ based on $D_r = 0.1$. More generally, Fig. S6 plots $m_k^{fragile}$ obtained from simulations for $D_r = 0.2, 0.1414, 0.1, 0.707, 0.05$. For $D_r < 10^{-1}$, we have performed a parabolic extrapolation to data in Fig. 1 and computed $m_k^{fragile}$ using Eq. (S1) based on the extrapolated values of D. The result shows an empirical relation $m_k^{fragile} \sim \ln D_r$. Extrapolating using this relation to $D_r = 10^{-14}$, we get $m_k^{fragile} = 120$, which is more consistent with the experimental range.

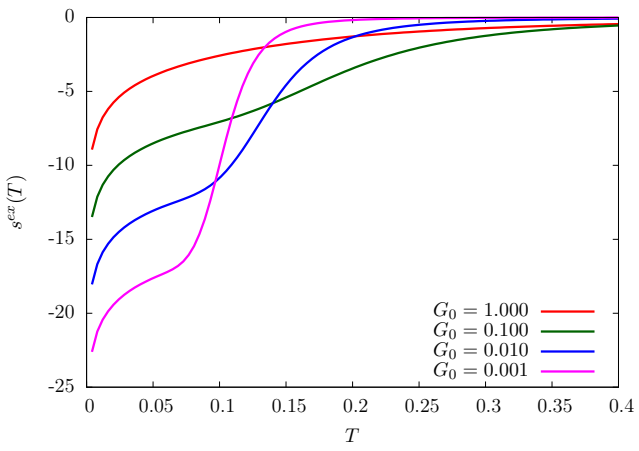

Figure S7. Excess entropy per particle s^{ex} against T at various G_0.

IV. ENTROPY CALCULATIONS

For the DPLM on the 2D square lattice with a small void density ϕ_v, the partition function in canonical ensemble can be shown to be given by [1]

$$Z = N!\mathcal{M}e^{-\beta N_b U}, \tag{S2}$$

where $\mathcal{M}$ is the number of possible particle occupation states and N_b denotes the average number of interacting pairs. Assuming isolated voids, we take $N_b \simeq 2N(1-\phi_v)$. From simple combinatorics, $\mathcal{M} = C(L^2, N_v)$, where $N_v = L^2\phi_v \simeq N\phi_v$ denotes the number of voids. Using $\ln n! \simeq n\ln n - n$, we get

$$\ln \mathcal{M} = N_v(\ln(L^2/N_v)+1) = N_v(1-\ln\phi_v). \tag{S3}$$

The Helmholtz free energy F follows $F = -k_BT\ln Z$. Using Eqs. (S2)-(S3), we get

$$F = N_bU - k_BTN_v(1-\ln\phi_v) - k_BTN(\ln N - 1) \tag{S4}$$

From the thermodynamic relation $F = E - TS$ with $E = N_b\overline{V}$, the entropy S is given by

$$S = \frac{N_b\left(\overline{V}-U\right)}{T} + Nk_B\phi_v\left(1-\ln\phi_v\right) + Nk_B\left(\ln N - 1\right), \tag{S5}$$

where we have defined

$$\mathcal{N} = \int e^{-V/k_BT}g(V)dV, \tag{S6}$$

$$\overline{V} = \frac{1}{\mathcal{N}}\int Ve^{-V/k_BT}g(V)dV, \tag{S7}$$

$$U = -k_BT\ln\int e^{-V/k_BT}g(V)dV. \tag{S8}$$

By defining entropy per particle as $s = S/N$, we further define an excess entropy per particle $s^{ex}(T) = s(T) - s^{LG}$ over the entropy $s^{LG} = k_B\phi_v(1-\ln\phi_v) + k_B(\ln N - 1)$ of a simple lattice gas [6]. Equation (S5) then gives

$$s^{ex} = \frac{2\left(1-\phi_v\right)\left(\overline{V}-U\right)}{T} \tag{S9}$$

Using Eq. (2) and after some straight-forward algebra, we get

$$s^{ex} = 2k_B(1-\phi_v)\Big\{1 + \ln\Big[(G_0/\Delta V)k_BT(1-e^{-\Delta V/k_BT}) + (1-G_0)e^{-\Delta V/k_BT}\Big] + \frac{[(1-G_0)\Delta V/k_BT - 1]}{(G_0/\Delta V)k_BT(e^{\Delta V/k_BT}-1) + (1-G_0)}\Big\}. \tag{S10}$$

Figure S7 shows the result for s^{ex} at $G_0 = 0.001, 0.01, 0.1$, and 1. As T decreases, a significant drop of s^{ex} occurs around $T \simeq 0.15$ and it becomes more and more dramatic as G_0 decreases.

This dramatic and controllable drop of s^{ex} around $T \simeq 0.15$ is the main cause of the high fragilities at small G_0. It results from a shift of the relative importance of the two components in $g(V)$. It can be intuitively understood by studying the interplay between the two components as follows. The bi-component $g(V)$ in Eq. (2) in the main text can be written as

$$g(V) = g_A(V) + g_B(V) \tag{S11}$$

where components labeled A and B are the uniform and Dirac distributions given by

$$g_A(V) = \frac{G_0}{\Delta V}, \tag{S12}$$

$$g_B(V) = (1-G_0)\delta(V-V_1). \tag{S13}$$

for $V \in [V_0, V_1]$ with $\Delta V = V_1 - V_0$. Generalizing Eqs. (S6)-(S9) to individual components, we write

$$\mathcal{N}_{A,B} = \int e^{-V/k_BT}g_{A,B}(V)dV, \tag{S14}$$

$$\overline{V}_{A,B} = \frac{1}{\mathcal{N}_{A,B}}\int Ve^{-V/k_BT}g_{A,B}(V)dV, \tag{S15}$$

$$U_{A,B} = -k_BT\ln\int e^{-V/k_BT}g_{A,B}(V)dV, \tag{S16}$$

$$s^{ex}_{A,B} = \frac{2\left(1-\phi_v\right)\left(\overline{V}_{A,B} - U_{A,B}\right)}{T}. \tag{S17}$$

which satisfy $\mathcal{N} = \mathcal{N}_A + \mathcal{N}_B$. These equations evaluate to

$$\mathcal{N}_A = \frac{G_0k_BT}{\Delta V}e^{-V_0/k_BT}(1-e^{-\Delta V/k_BT}), \tag{S18}$$

$$\overline{V}_A = V_0 + k_BT - \frac{\Delta V}{e^{\Delta V/k_BT}-1}, \tag{S19}$$

$$U_A = V_0 - k_BT\ln\left[\frac{G_0k_BT}{\Delta V}\left(1-e^{-\Delta V/k_BT}\right)\right], \tag{S20}$$

$$s^{ex}_A = 2k_B\left(1-\phi_v\right)\left\{1 + \ln\left[\frac{G_0k_BT}{\Delta V}\left(1-e^{-\Delta V/k_BT}\right)\right] - \frac{\Delta V}{k_BT}\frac{1}{e^{\Delta V/k_BT}-1}\right\}, \tag{S21}$$

and

$$\mathcal{N}_B = (1-G_0)e^{-(V_0+\Delta V)/k_BT}, \tag{S22}$$
$$\overline{V}_B = V_0 + \Delta V, \tag{S23}$$
$$U_B = V_0 + \Delta V - k_BT\ln(1-G_0), \tag{S24}$$
$$s_B^{ex} = 2k_B(1-\phi_v)\ln(1-G_0). \tag{S25}$$

Then, s^{ex} can alternatively be calculated using the standard expression for two-state systems:

$$s^{ex} = Xs_A^{ex} + (1-X)s_B^{ex} - Xk_B\ln X - (1-X)k_B\ln(1-X), \tag{S26}$$

where $X = \mathcal{N}_A/\mathcal{N}$ is the probabilistic weight of component A. In Eq. (S26), the first two terms are the contributions of the two components. The remaining terms are the entropy due to the mixing of the components, which approaches 0 for X approaching 0 or 1. Equation (S26) also evaluates to Eq. (S10) after some algebra.

For $G_0 \ll 1$ corresponding to the regime relevant to fragile glasses, component A corresponds to the low energy states important at low T while the component B corresponds to the numerous states important at high T. Mathematically, as T decreases, X increases from 0 to 1. Therefore, Eqs (S26), (S21) and (S25) give

$$s^{ex} \to \begin{cases} 0 & \text{for } T\to\infty \\ s_A^{ex} & \text{for } T\to 0 \end{cases} \tag{S27}$$

where

$$s_A^{ex} = 2k_B(1-\phi_v)\left[1+\ln\left(\frac{G_0k_BT}{\Delta V}\right)\right] \quad \text{for } T\to 0, \tag{S28}$$

and we have considered $k_BT \ll \Delta V$ for simplicity. At small G_0, due to the $\ln G_0$ dependence, s^{ex} at low T, for which the main contribution is s_A^{ex}, is small. This explains the dramatic drop from 0 as T decreases at small G_0.

Note that the bi-component $g(V)$ considered here is fully analogous to a two-state model of glass proposed in Ref. [7], which considers microscopic states suggested as particle bonds taking either a low-entropy unexcited state or a high-entropy excited state. Although our component A is a band of states, the energy spread becomes narrow at low T and this contributes to the similarity between the models. In Ref. [7], the entropy difference ΔS^0 and the enthalpy difference ΔH^0 between excited and unexcited state are the fitting parameters for the entropy for different materials. In our model, we can now compute ΔS^0 and ΔH^0. By dividing Eqs. (S21) and (S25) by $2(1-\phi_v)$, we get the extropy per bond for the unexcited and excited state respectively. The entropy difference ΔS^0 is then $\Delta S^0 = (s_B^{ex} - s_A^{ex})/[2(1-\phi_v)]$, which gives

$$\Delta S^0 = k_B\left\{\ln\left[\frac{(1-G_0)}{G_0(1-e^{-\Delta V/k_BT})}\frac{\Delta V}{k_BT}\right] + \frac{\Delta V}{k_BT}\frac{1}{e^{\Delta V/k_BT}-1} - 1\right\}. \tag{S29}$$

On the other hand, ΔH^0 is simply given by $\Delta H^0 = \overline{V}_B - \overline{V}_A$. Using Eqs. (S19) and (S23),

$$\Delta H^0 = k_BT\left[\frac{\Delta V}{k_BT}\left(1+\frac{1}{e^{\Delta V/k_BT}-1}\right) - 1\right]. \tag{S30}$$

For the fragile glass with $G_0 = 0.01$ and $E_0 = 0$, our DPLM simulations give $T_g \simeq 0.163$. Noting that $k_B = \Delta V = 1$, Eqs. (S29) and (S30) give $\Delta S^0/k_B = 5.42$ and $\Delta H^0/k_BT_g = 5.15$ at $T = T_g$. This can be compared with the fragile glass of toluene for example. By fitting to experimental results on entropy measurements, the two state model gives $\Delta S^0 = 45.4$ J/mol·K and $\Delta H^0 = 6760$ J/mol, expressed in terms of per mole of excitable states [7]. Taking $k_B = 8.315$ J/mol·K and $T_g = 117$ K, they lead to $\Delta S^0/k_B = 5.46$ and $\Delta H^0/k_BT_g = 6.95$. Toluene is considered because this value of $\Delta S^0/k_B$ matches the value 5.42 from DPLM simulations. The consistency of the value of $\Delta H^0/k_BT_g$ with the DPLM result of 5.15 then provides an additional support of the close relation between the two state model and the DPLM with the bi-component form of $g(V)$.

[1] L.-H. Zhang and C.-H. Lam, "Emergent facilitation behavior in a distinguishable-particle lattice model of glass," Phys. Rev. B **95**, 184202 (2017).

[2] M. Matthieu, "Relaxation and physical aging in network glasses: a review," Rep. Prog. Phys. **79**, 066504 (2016).

[3] C.-H. Lam, "Local random configuration-tree theory for string repetition and facilitated dynamics of glass," J. Stat. Mech. **2018**, 023301 (2018).

[4] C. A. Angell, "Relaxation in liquids, polymers and plastic crystals strong/fragile patterns and problems," J. Non-Cryst. Solids **131-133**, 13 (1991).

[5] C. Alba, L. E. Busse, D. J. List, and C. A. Angell, "Thermodynamic aspects of the vitrification of toluene, and xylene isomers, and the fragility of liquid hydrocarbons," J. Chem. Phys. **92**, 617 (1990).

[6] J. C. Dyre, "Perspective: Excess-entropy scaling," J. Chem. Phys. **149**, 210901 (2018).

[7] C. T. Moynihan and C. A. Angell, "Bond lattice or excitation model analysis of the configurational entropy of molecular liquids," J. Non-Cryst. Solids **274**, 131 (2000).